Supplementary Note

Prkcsh and Sec63 mutant phenotypes: Null alleles for Sec63 and Prkcsh were produced by intercrossing the respective conditional *Prkcsh*^{flox} and *Sec63*^{flox} alleles with the ACTB-Cre deleter mice. Mice heterozygous for the deleted alleles were intercrossed and embryos were examined at E7.5, E9.5, E11.5 and E12.5. *Prkcsh*$^{-/-}$ embryos die *in utero* by embryonic day E11.5. *Sec63*$^{-/-}$ embryos were not found at any of the above time points, suggestive of very early lethality.

We next examined tissue selective inactivation of the conditional alleles for each gene. Kidney selective *Prkcsh*$^{flox/flox}$*;Ksp-Cre* knockout mice have mild microscopic cystic disease at P28, cystic disease as shown in Fig. 1C at P42, more advanced cystic disease at 3 months and severe disease with increasing mortality by 6 months. *Sec63*$^{flox/flox}$*;Ksp-Cre* kidney selective knockouts have mild microscopic cystic disease at P14, cystic disease as shown in Fig. 2A at P21, more advanced cystic disease at P30 and severe disease with increasing mortality by P60. For both *Prkcsh* and *Sec63* models, tamoxifen inducible inactivation in adult mice beginning at P28 produced bile duct-derived cysts in the liver by 8 weeks following tamoxifen treatment. This mild to moderate cystic disease is shown for *Prkcsh* in Fig. 1B (data not shown for *Sec63*); severe cystic liver disease was present by 4-5 months following induction. Higher dose tamoxifen induction regimens using the generalized *pCX-CreER* is acutely fatal in both *Prkcsh* and *Sec63* lines. Across all Cre lines examined and across all cystic phenotypes, *Sec63* is consistently more severe than *Prkcsh*. The time points chosen for the analyses in the current study were based on the above investigations and chosen to provide reproducible intermediate cystic phenotypes for which both worsening and improvement can be readily discerned.

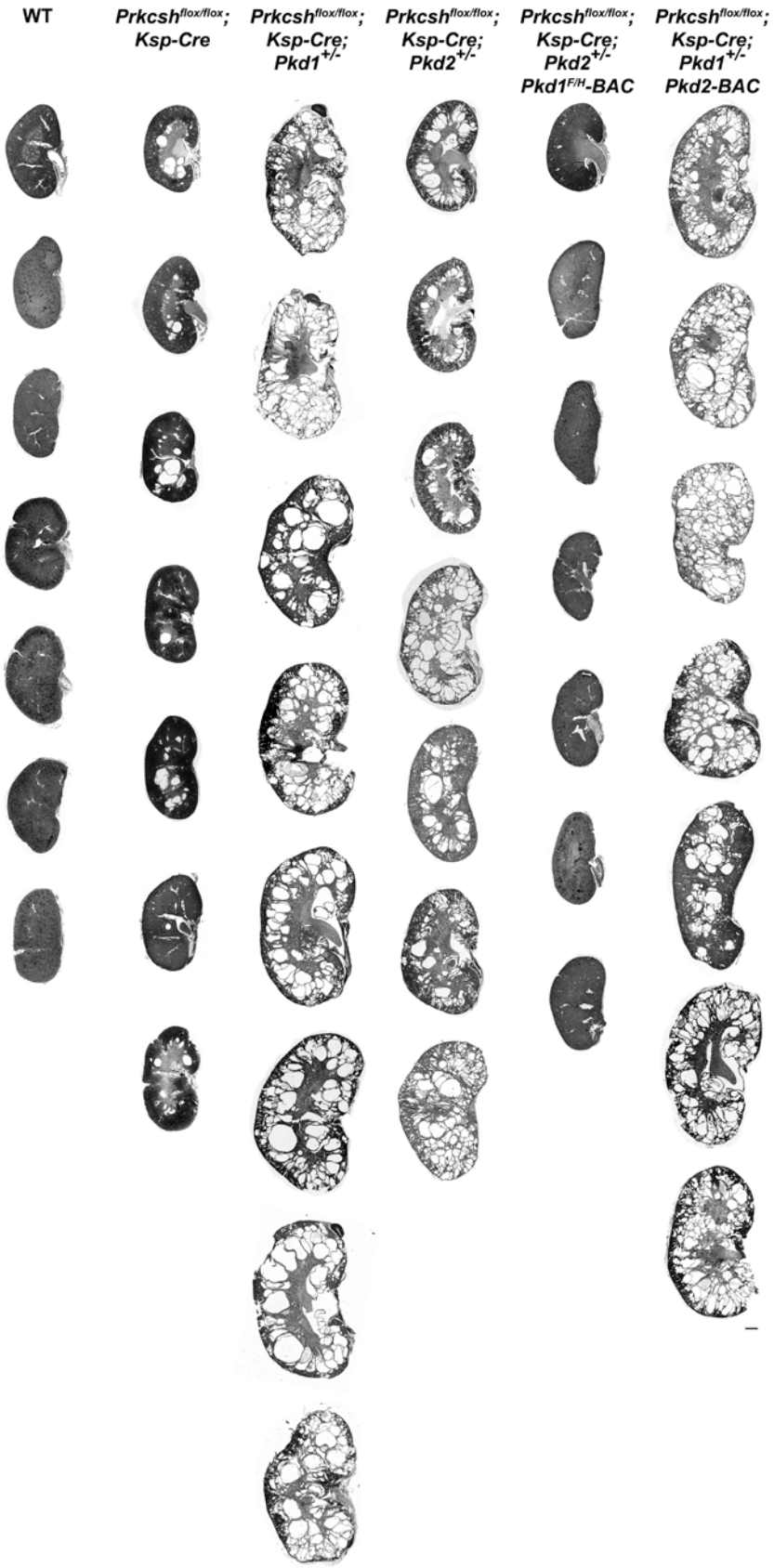

Supplementary Figure 1. Histology of all mice used to examine the genetic interaction between *Prkcsh* and *Pkd1/Pkd2* (Fig. 1B).
The top row corresponds to the images used in Fig. 1A. Scale bar, 1 mm.

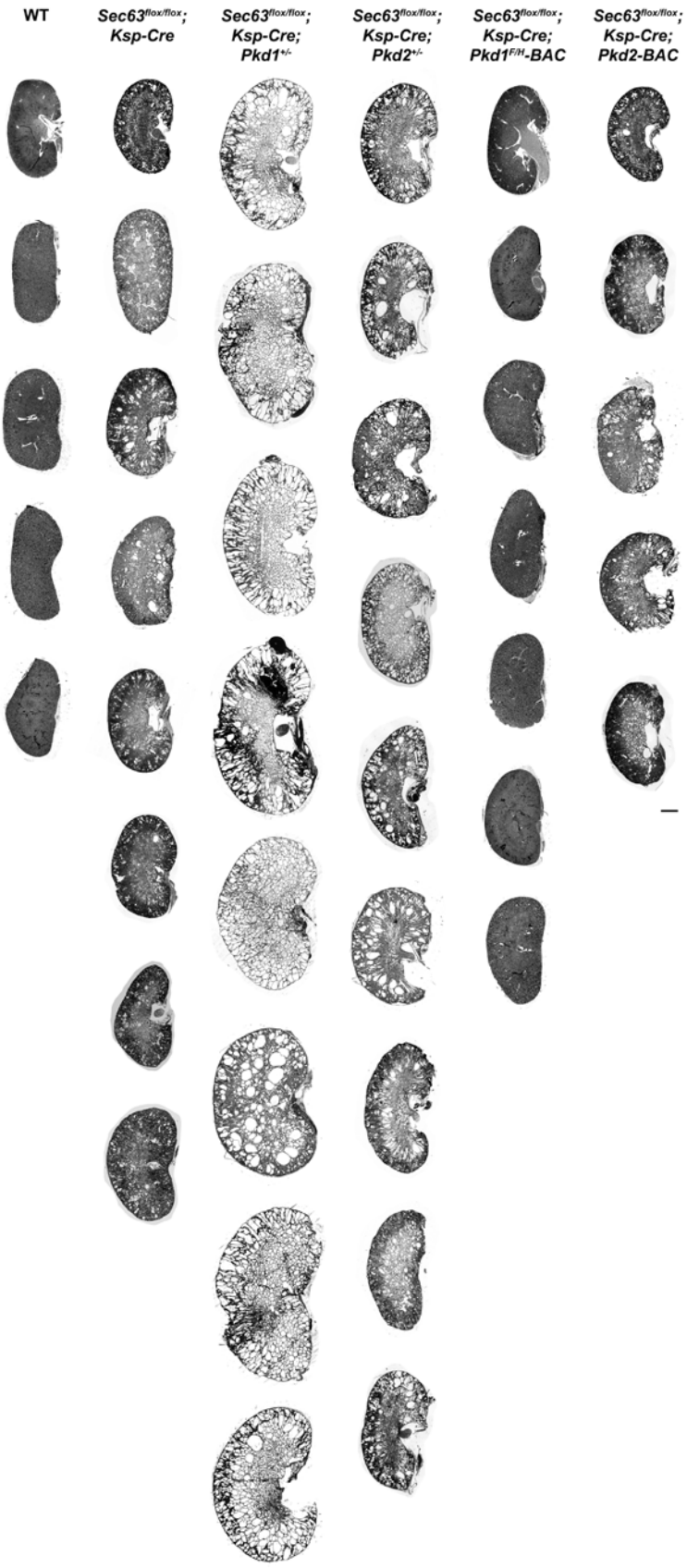

Supplementary Figure 2. Histology of all mice used to examine the genetic interaction between *Sec63* and *Pkd1/Pkd2* (Fig. 2B).
The top row corresponds to the images used in Fig. 2A. Scale bar, 1 mm.

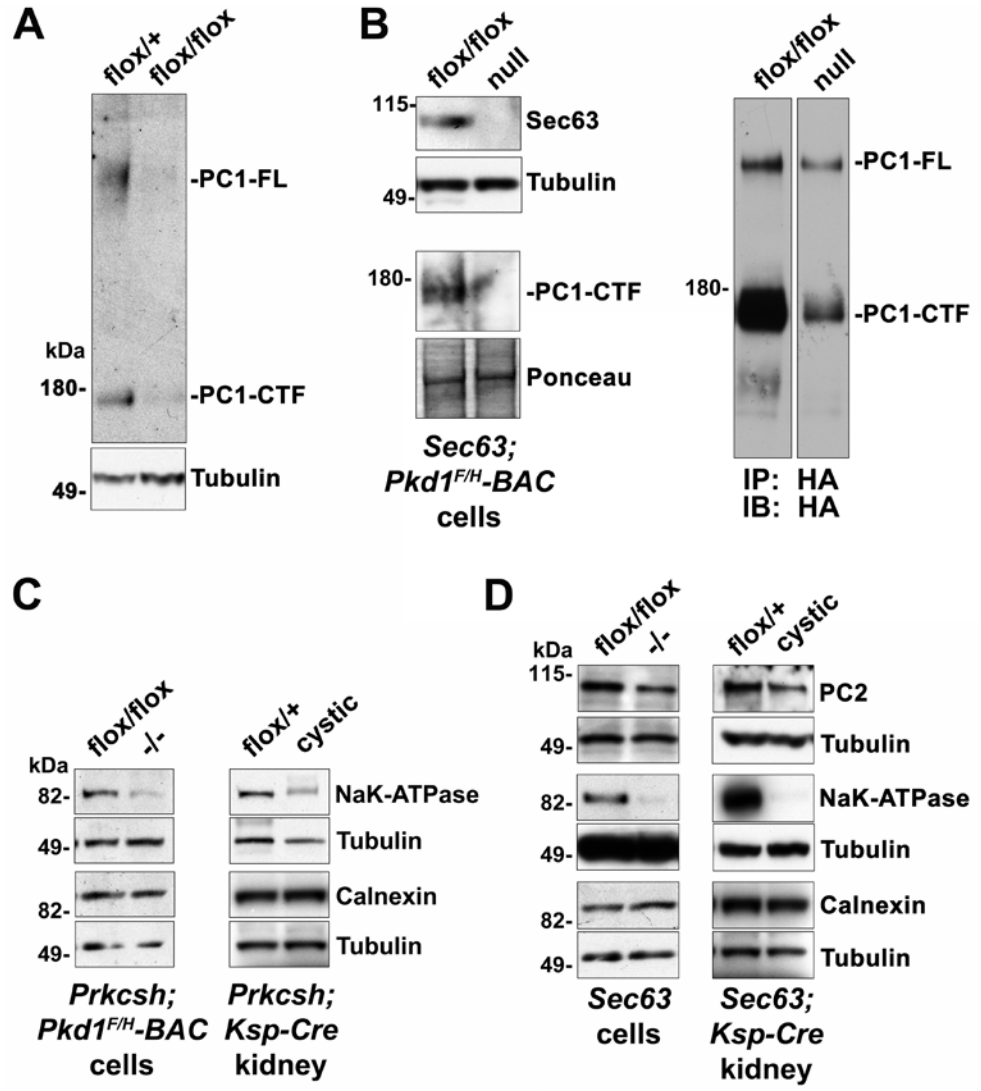

Supplementary Figure 3. Generalized defects in expression of integral membrane proteins resulting from ADPLD gene mutations.

(**A**) Immunoblot of kidney tissue lysates from P7 *Prkcsh*$^{flox/+}$*;Ksp-Cre;Pkd1*$^{F/H}$*-BAC* (flox/+) and *Prkcsh*$^{flox/flox}$*;Ksp-Cre;Pkd1*$^{F/H}$*-BAC* (flox/flox) mice. PC1-FL and PC1-CTF detected by anti-HA showing reduced PC1 expression following homozygous inactivation of *Prkcsh*. (**B**) Sec63p expression is present in *Sec63*$^{flox/flox}$*;Pkd1*$^{F/H}$*-BAC* cells (*flox/flox*) but is absent in *Sec63*$^{-/-}$*;Pkd1*$^{F/H}$*-BAC* cell lines (*null*) following transient Cre expression (*upper left panels*). Whole-cell lysates show decreased expression of PC1-CTF detected by anti-HA in null cells (*lower left panels*). Ponceau red staining of a non-specific protein band serves as loading control. *Rght panel*, two lanes from a single immunoblot of following immunoprecipitation and immunblotting by anti-HA showing reduction in both the intramembranous PC1-CTF and uncleaved full length PC1 (PC1-FL) in Sec63 null cells. (**C**) Representative immunoblots from *Prkcsh*$^{-/-}$*;Pkd1*$^{F/H}$*-BAC* cells lines compared to *Prkcsh*$^{flox/flox}$*;Pkd1*$^{F/H}$*-BAC* controls (*left panel*) and mosaic 2.5 month-old *Prkcsh*$^{flox/flox}$*;Ksp-Cre* cystic kidney tissue compared to *Prkcsh*$^{flox/+}$*;Ksp-Cre* non-cystic controls (*right panel*) showing reduced expression of the α subunit of the NaK-ATPase in both cells and tissue. Expression of the ER membrane protein calnexin is unchanged. Tubulin serves as a loading control. (**D**) Representative immunoblots from *Sec63*$^{-/-}$ cells lines compared to *Sec63*$^{flox/flox}$ controls (*left panel*) and mosaic 1 month-old *Sec63*$^{flox/flox}$*;Ksp-Cre* (cystic)kidney tissue compared to *Sec63*$^{flox/+}$*;Ksp-Cre* (flox/+) non-cystic controls (*right panel*). PC2 is moderately reduced in both knockout cells and cystic tissue whereas NaK-ATPase is markedly reduced in knockout cells and mutant tissue. As with GIIβ, expression of the ER membrane protein calnexin is unchanged. Tubulin serves a loading control.

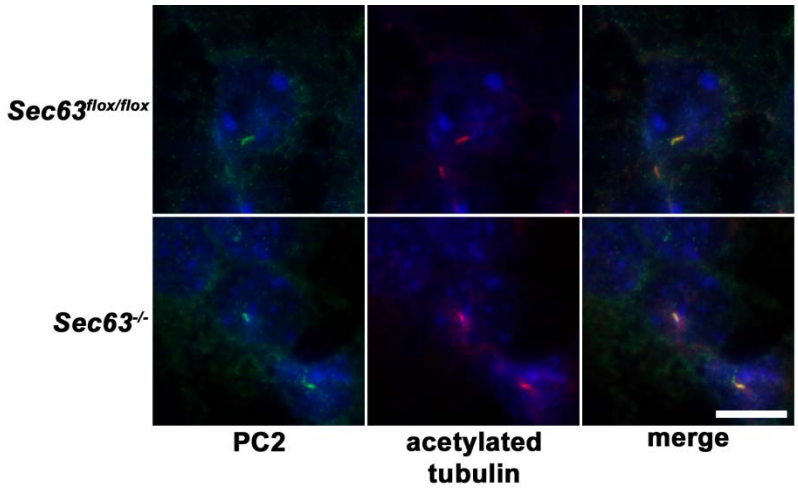

Supplementary Figure 4. PC2 expression in cilia of *Sec63*$^{-/-}$ cells.
PC2 trafficking to cilia is not altered by loss of Sec3 (*bottom*). Green, anti-PC2 (YCC2); red, acetylated α-tubulin. Scale bar, 5 μm.

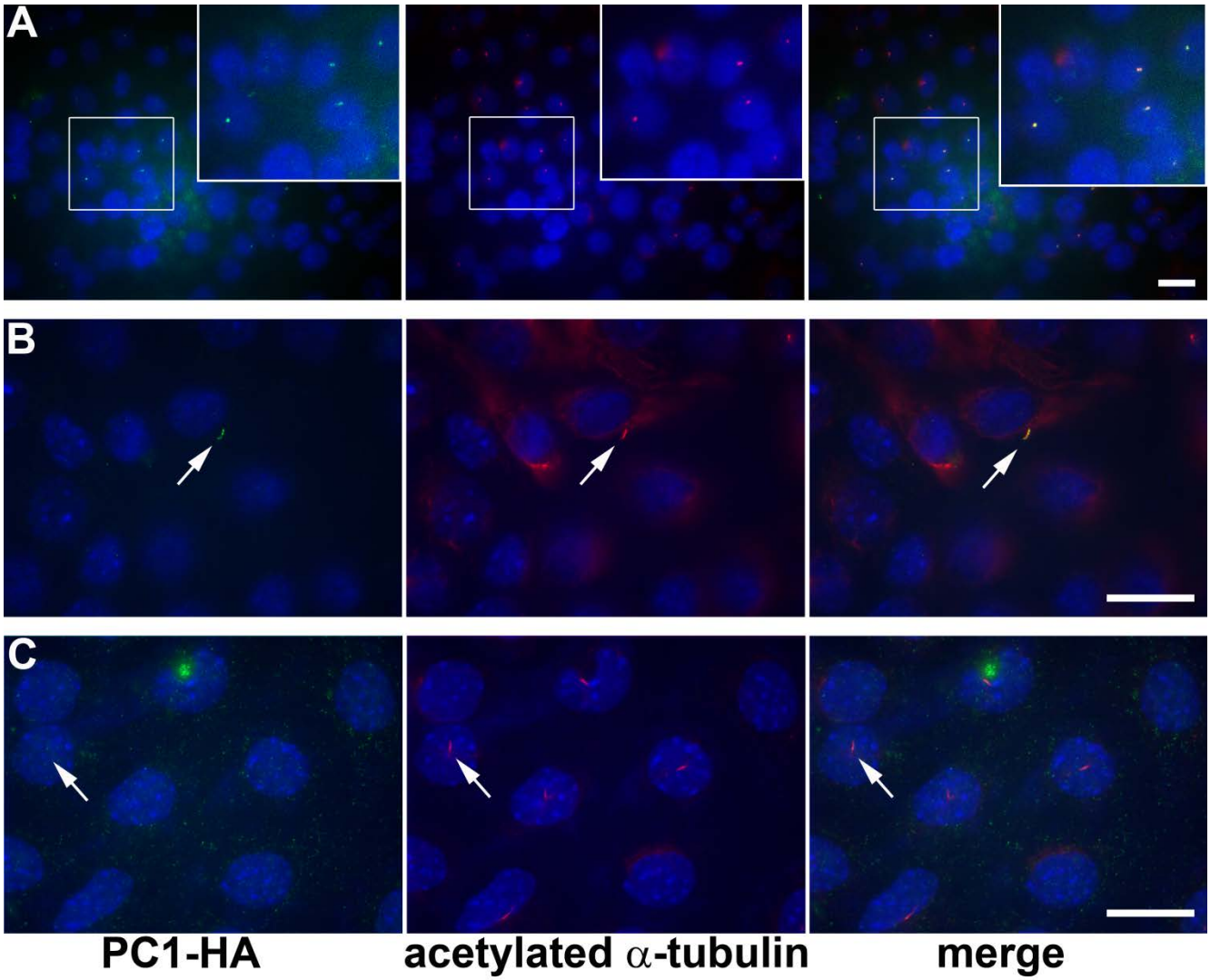

Supplementary Figure 5. Defective PC1 trafficking to cilia in *Prkcsh* mutant cells. This figure serves to illustrate that the differences in cilia trafficking of PC1 between *Prkcsh*$^{flox/flox}$;*Pkd1*$^{F/H}$-*BAC* cells and *Prkcsh*$^{-/-}$;*Pkd1*$^{F/H}$-*BAC* cells shown in Fig. 3E, F is a general property of the respective cell populations. (**A**) A lower magnification image of the ciliary localization of PC1 in *Prkcsh*$^{flox/flox}$;*Pkd1*$^{F/H}$-*BAC* cells. PC1 is readily detectable by anti-HA staining (green) in several ciliated cells in the field. Boxed region is digitally magnified x2 in the inset. Acetylated α-tubulin (red) marks cilia. Scale bar, 10 μm. (**B**) Lower power field of the same image used in Fig. 3F, *top panels*, showing *Prkcsh*$^{flox/flox}$;*Pkd1*$^{F/H}$-*BAC* cells with a single cilium positive for PC1. Arrow points to cilium shown in Fig. 3F. Scale bar, 10 μm. (**C**) Lower power field of the same image used in Fig. 3F, *bottom panels*, showing *Prkcsh*$^{-/-}$;*Pkd1*$^{F/H}$-*BAC* cells with several cilia negative for PC1. Arrow points to cilium shown in Fig. 3F. Scale bar, 10 μm.

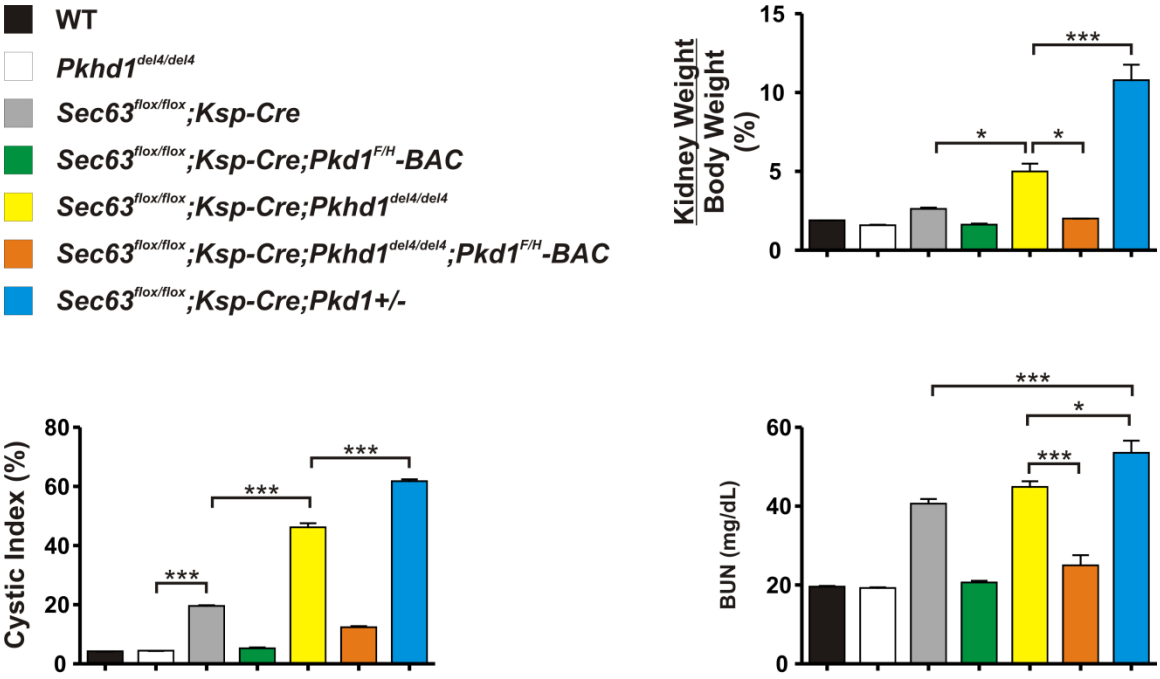

Supplementary Figure 6. Reduced dosage of *Pkd1* results in more severe cystic disease than reduced dosage of *Pkhd1* in *Sec63$^{flox/flox}$;Ksp-Cre* mice.

Combined data from Figs. 2B and 6B analyzed together by ANOVA showing that the severity of cystic disease by three parameters is greater in *Sec63$^{flox/flox}$;Ksp-Cre;Pkd1$^{+/-}$* mice (blue) than *Sec63$^{flox/flox}$;Ksp-Cre;Pkhd1$^{del4/del4}$* mice (yellow). *n* (from left to right)=5, 6, 8, 7, 6, 6, 8; ***, $P<0.001$, *, $P<0.05$

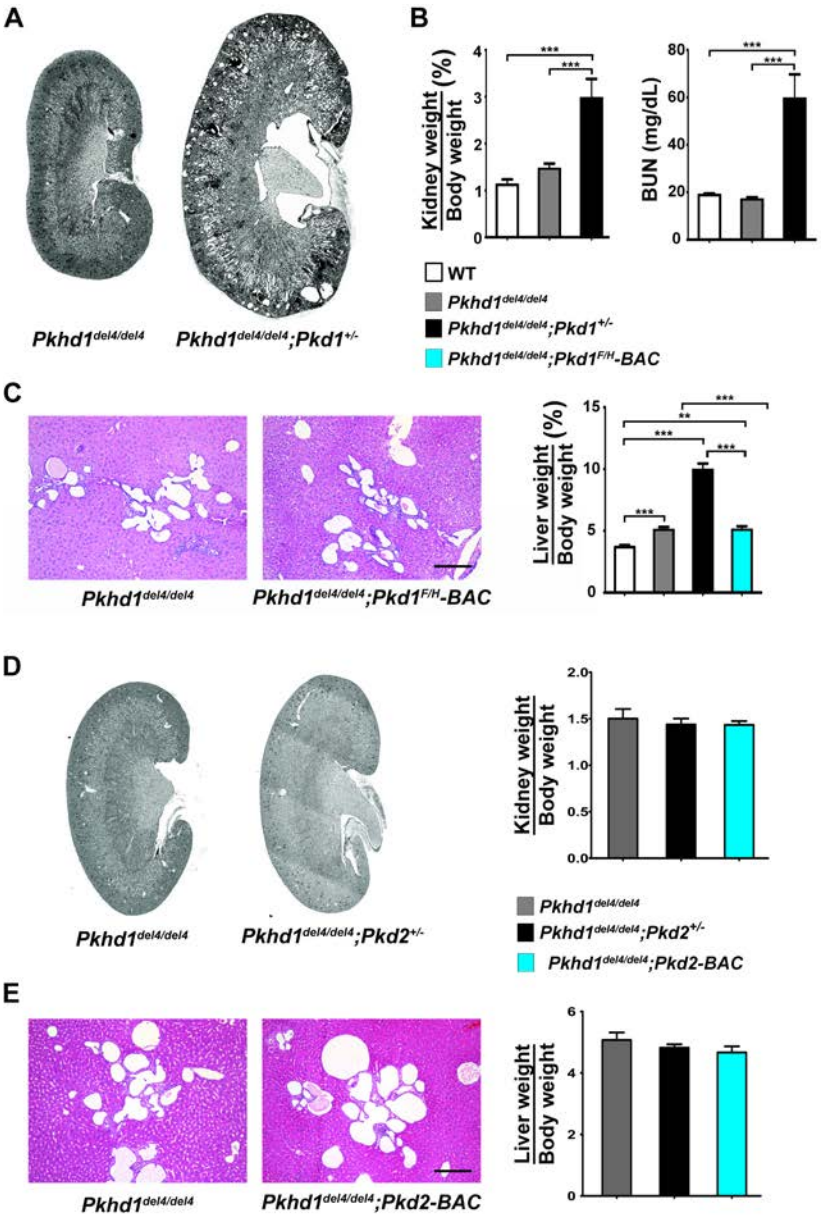

Supplementary Figure 7: Genetic interaction between *Pkd1* and *Pkhd1*.
(**A**) Representative images of kidneys from *Pkhd1*$^{del4/del4}$ and *Pkhd1*$^{del4/del4}$;*Pkd1*$^{+/-}$ mice at six months showing the occurrence radially arrayed fusiform tubular dilation on the *Pkd1*$^{+/-}$ background. *Pkhd1*$^{del4/del4}$ kidneys are no cystic. (**B**) Kidney weight to body weight ratio is significantly increased in the *Pkhd1*$^{del4/del4}$;*Pkd1*$^{+/-}$ six month old animals (n=4) compared to age matched wild-type (n=8) and *Pkhd1*$^{del4/del4}$ (n=13) mice. Kidney function as assessed by blood urea nitrogen (BUN) was impaired in the *Pkhd1*$^{del4/del4}$;*Pkd1*$^{+/-}$ mice (n=3) compared to wild-type (n=7) and *Pkhd1*$^{del4/del4}$ mice (n=13). (**C**) Representative liver sections showing absence of improvement in the liver phenotype in *Pkhd1*$^{del4/del4}$ mice upon *Pkd1*$^{F/H}$-*BAC* expression. Scale bar, 500 μm. Aggregate data on liver weight/body weight ratio shows that *Pkhd1*$^{del4/del4}$;*Pkd1*$^{+/-}$ (n=4) have significantly increased liver size compared to the *Pkhd1*$^{del4/del4}$ alone (n=13), which in turn was significantly increased compared to wild type control (n=12). The addition of the *Pkd1*$^{F/H}$-*BAC* transgene on the *Pkhd1*$^{del4/del4}$ background (n=7) did not rescue the *Pkhd1*$^{del4/del4}$ liver phenotype. ***, P<0.001; **, P<0.01. (**D, E**) *Pkd2* does not interact with *Pkhd1*. Representative images of kidneys (**D**) and livers (**E**) from mice with the indicated genotypes at six months. Aggregate data for kidney weight to body weight ratio (**D**) and liver weight to body weight ratio (**E**) at six months is no different between *Pkhd1*$^{del4/del4}$ (n=13), *Pkhd1*$^{del4/del4}$;*Pkd2*$^{+/-}$ (n=9) and, *Pkhd1*$^{del4/del4}$;*Pkd2-BAC* (n=5) mice. Scale bar, 500 μm.

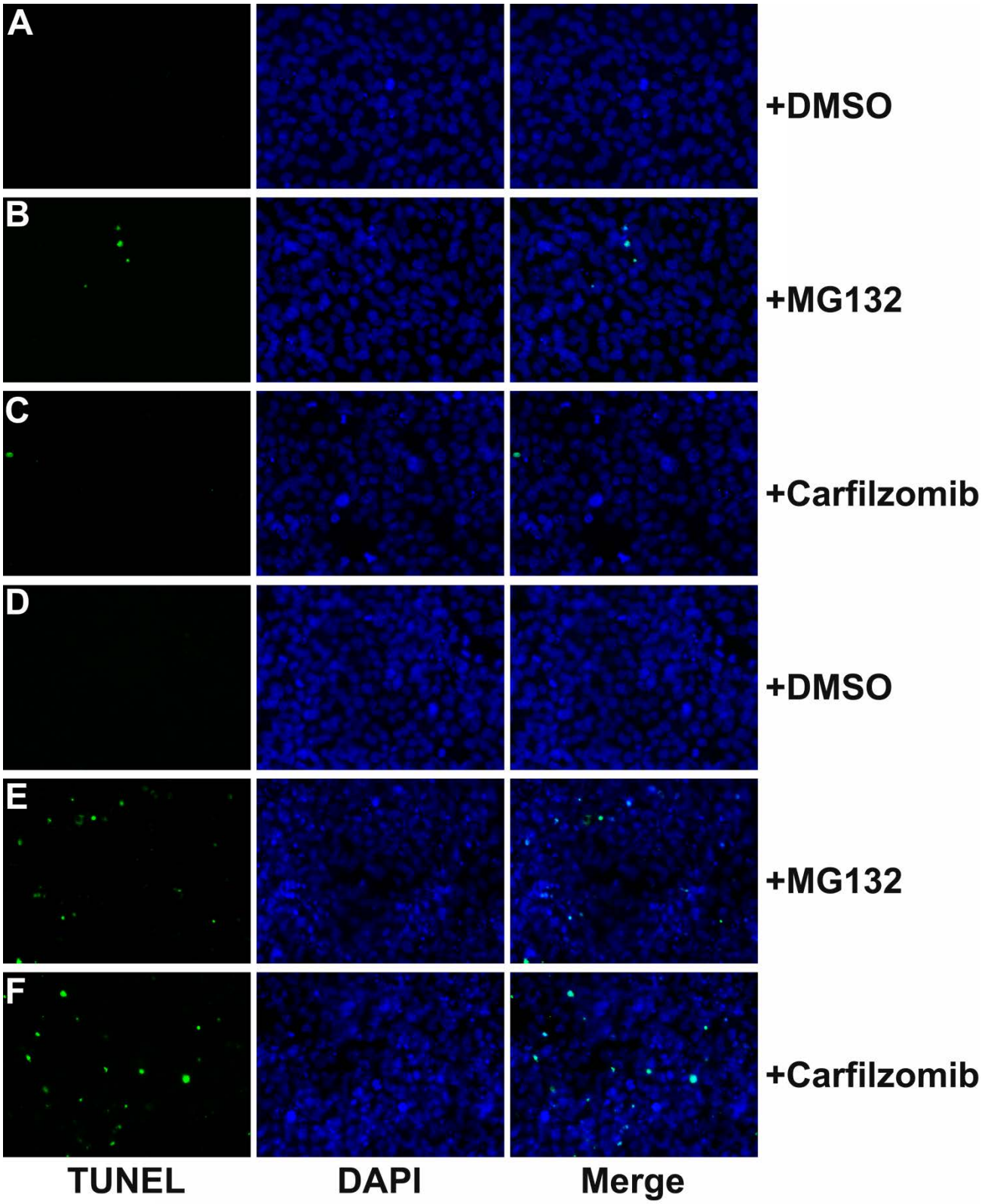

Supplementary Figure 8. *Prkcsh* mutant cells show increased apoptosis in response to proteasome inhibition.

Representative images of (**A-C**) *Prkcsh*$^{flox/flox}$ cells and (**D-F**) *Prkcsh*$^{-/-}$ cells treated with DMSO or the proteasome inhibitors MG132 (20 μM) or carfilzomib (130 nM). Sensitivity to these treatments was evaluated by determining the rates of apoptosis by TUNEL staining (green). Scale bar, 20 μm. Quantitation of apoptosis by genotype and treatment is provided in Fig. 7A.

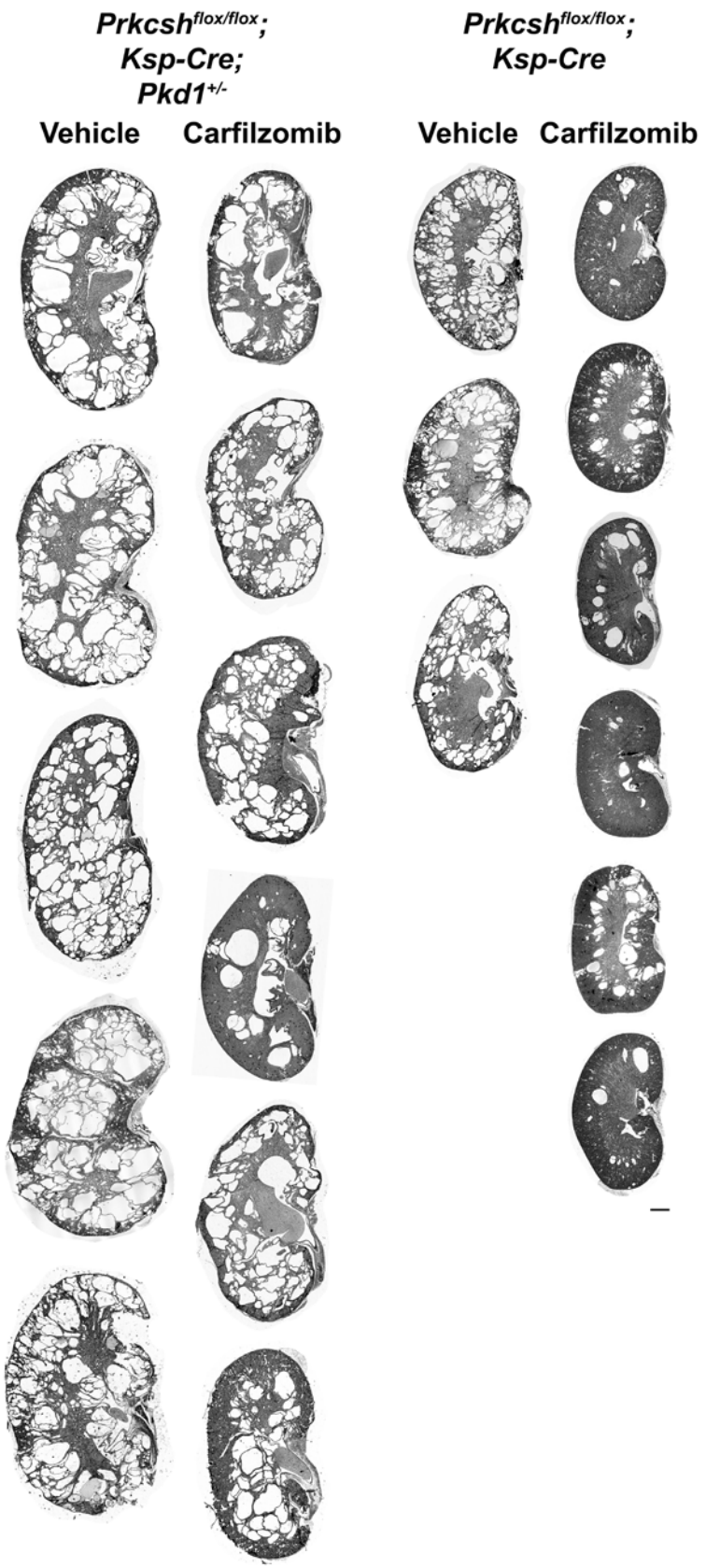

Supplementary Figure 9. Histology of all mice used to examine the effects of proteasome inhibition on the course of ADPLD (Fig. 7C-F).
The top row corresponds to the genotypes used in Fig. 7C, D. Scale bar, 1 mm.